Ultrasound in Med. & Biol., Vol. 24, No. 9, pp. 1419–1435;1998

0301-5629/98/$–see front matter

PII S0301-5629(98)00110-0

● *Original Contribution*

SHEAR WAVE ELASTICITY IMAGING: A NEW ULTRASONIC TECHNOLOGY OF MEDICAL DIAGNOSTICS

ARMEN P. SARVAZYAN,* OLEG V. RUDENKO,† SCOTT D. SWANSON,‡ J. BRIAN FOWLKES,‡ and STANISLAV Y. EMELIANOV§

*Artann Laboratories, East Brunswick, NJ; †Department of Acoustics, Moscow State University, Moscow, Russia; ‡Department of Radiology, University of Michigan Medical Center, Ann Arbor, MI; and §Biomedical Engineering Department, University of Michigan, Ann Arbor, MI

(*Received* 5 *September* 1997; *in final form* 2 *July* 1998)

Abstract—Shear wave elasticity imaging (SWEI) is a new approach to imaging and characterizing tissue structures based on the use of shear acoustic waves remotely induced by the radiation force of a focused ultrasonic beam. SWEI provides the physician with a virtual "finger" to probe the elasticity of the internal regions of the body. In SWEI, compared to other approaches in elasticity imaging, the induced strain in the tissue can be highly localized, because the remotely induced shear waves are attenuated fully within a very limited area of tissue in the vicinity of the focal point of a focused ultrasound beam. SWEI may add a new quality to conventional ultrasonic imaging or magnetic resonance imaging. Adding shear elasticity data ("palpation information") by superimposing color-coded elasticity data over ultrasonic or magnetic resonance images may enable better differentiation of tissues and further enhance diagnosis. This article presents a physical and mathematical basis of SWEI with some experimental results of pilot studies proving feasibility of this new ultrasonic technology. A theoretical model of shear oscillations in soft biological tissue remotely induced by the radiation force of focused ultrasound is described. Experimental studies based on optical and magnetic resonance imaging detection of these shear waves are presented. Recorded spatial and temporal profiles of propagating shear waves fully confirm the results of mathematical modeling. Finally, the safety of the SWEI method is discussed, and it is shown that typical ultrasonic exposure of SWEI is significantly below the threshold of damaging effects of focused ultrasound. © **1998 World Federation for Ultrasound in Medicine & Biology.**

Key Words: **Elasticity imaging, Ultrasound imaging, Shear elastic modulus, Magnetic resonance imaging, Shear wave elasticity imaging, Nonlinear acoustics, Radiation pressure, Tissue differentiation.**

INTRODUCTION

Shear wave elasticity imaging (SWEI) is a new approach to imaging and characterizing tissue structures based on the use of shear acoustic waves remotely induced by the radiation force of a focused ultrasonic beam. SWEI emerged a few years ago, and certain aspects of SWEI are described by Sarvazyan (1995a), Rudenko et al. (1996), Andreev et al. (1996, 1997a, 1997b), Sarvazyan (1997), Emelianov et al. (1997), and Sarvazyan and Rudenko (1997). SWEI may be considered a new way of realizing the idea of "elasticity imaging" or "elastography" being developed in a number of laboratories around the world (Cespedes et al. 1993; Emelianov et al. 1995; Fowlkes et al. 1995; Krouskop et al. 1987; Lerner et al. 1990; O'Donnell et al. 1994; Ophir et al. 1991, 1996; Parker et al. 1990; Skovoroda et al. 1994, 1995; Yamakoshi et al. 1990).

Elasticity imaging adds a new quality to conventional diagnostic ultrasound: it enables differentiation of tissues based on their hardness, thereby enhancing the contrast in the image and revealing anatomical structures composed of tissues with different shear moduli. Compared to many other tissue characterization parameters used in various imaging modalities, such as ultrasound, magnetic resonance imaging (MRI), positron emission tomography, and computed tomography, elasticity represents a property that is most easy to grasp and interpret. An image based upon elasticity intrinsically answers a very natural question of the physician: "is the region of interest hard or soft?" Elasticity imaging provides the physician with a virtual "finger," enabling him or her to probe internal regions of the body to determine their physical characteristics.

Address correspondence to: Armen P. Sarvazyan, Artann Laboratories, Inc., 1735 Linvale-Harbourton Road, Lambertville, NJ 08530-3302, USA. E-mail: armen@pluto.njcc.com

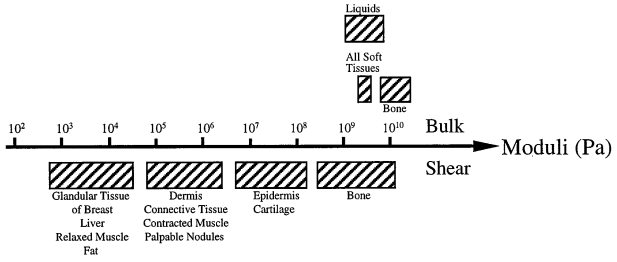

Fig. 1. Summary of data from the literature concerning the variation of the shear and bulk moduli for various materials and body tissues. Ranges associated with each modulus for a given tissue type are indicated by the shaded regions.

It is instructive to compare the physical bases for detecting tissue lesions by different diagnostic techniques. The diagnostic value of a characteristic of a tissue depends upon the range of variation of that characteristic as a function of the state of the tissue (Sarvazyan et al. 1995b). The ability of ultrasound imaging to differentiate various tissues within the body depends principally upon the acoustic impedance, which in turn depends upon the bulk elasticity modulus of the tissue under examination. Inspection of Fig. 1 reveals that, for soft tissues, the range of variation of the bulk modulus is significantly less than an order of magnitude (Frizzell et al. 1976; Goss et al. 1978; Sarvazyan et al. 1995b). However, the "hardness" or "elasticity" of tissue sensed by palpation reflects the value of the shear modulus, which, for soft tissues, as shown in Fig. 1, varies over several orders of magnitude (Sarvazyan 1975; Sarvazyan et al. 1995b). The data presented in Fig. 1 argue persuasively for seeking a technique in which the shear elasticity is used to characterize tissues. The utilization of this great unexploited potential is the main objective of the efforts to investigate possibilities of medical imaging with the use of shear waves.

This article presents a physical and mathematical basis of SWEI with some experimental results of pilot studies proving the feasibility of this new ultrasonic technology of medical imaging and diagnostics.

GENERAL PRINCIPLES OF SHEAR WAVE ELASTICITY IMAGING

The core of the SWEI method is shear wave generation by radiation force produced by an amplitude-modulated beam of focused ultrasound. These remotely induced waves subsequently are detected using an appropriate imaging modality. The information then is analyzed and the tissue viscoelastic properties are evaluated. In SWEI, compared to other approaches in elasticity imaging, the induced strain in the tissue can be highly localized, because the remotely induced shear waves are attenuated fully within a few wavelengths distance. By choosing the proper modulation frequency (typically in the low kHz range), the wavelength of shear waves can be adjusted to minimize the influence of the tissue boundaries. The very large attenuation of shear waves, as compared with compressional waves where attenuation is two to three orders of magnitude less, is the main reason that shear waves have been ignored as a possible means of obtaining information about the mechanical properties of tissue. Interestingly, this unfavorable feature of shear waves is one of the factors providing the feasibility of SWEI. Due to the high attenuation of shear waves, it is possible to induce mechanical oscillations within a very limited area of tissue in the vicinity of the focal point of a focused ultrasound beam.

To explain a basic principles of the shear wave elasticity imaging, Fig. 2 shows a schematic diagram of SWEI in general form. The excitation focused transducer (ultrasonic phased array or a single focused transducer) is used to generate remote shear waves. This shear wave propagates through the tissue and is detected. Various possibilities of detection of a remotely induced shear wave also are shown in Fig. 2.

The detection of generated shear waves can be done using either the same excitation transducer or other independent ultrasound pulse-echo imaging transducers (Andreev et al. 1996, 1997a, 1997b; Sarvazyan et al. 1995c). First, the same transducer array can be used for shear wave excitation, then for shear wave detection, and, finally, for imaging of tissue structures. This greatly facilitates the task of designing elasticity imaging devices. The imaging transducer also can be incorporated into the excitation transducer used for shear wave generation (Sarvazyan et al. 1995c). This may be a useful design for applications, such as elasticity imaging of brain, which have limited acoustic access to the object. For other applications, such as breast elasticity imaging, the imaging transducer can be positioned on the other side of the imaged tissue. Finally, other locations of the imaging ultrasound transducer are also possible, as illustrated in Fig. 2.

Another possible realization of SWEI is detection of ultrasonically induced shear waves at the surface of the tissue using low-frequency acoustic detectors. In this case, the modulation parameters of the focused ultrasound beam should be chosen such that a detectable fraction of the shear wave energy can reach the surface of the tissue. This realization of SWEI is similar to that widely used in geophysics, where surface detection of waves generated by deep underground explosions is used to image geological structures. Processing the signals that passed through a heterogeneous medium and solving the inverse problem, it is possible to reconstruct the geometric and mechanical features of the medium.

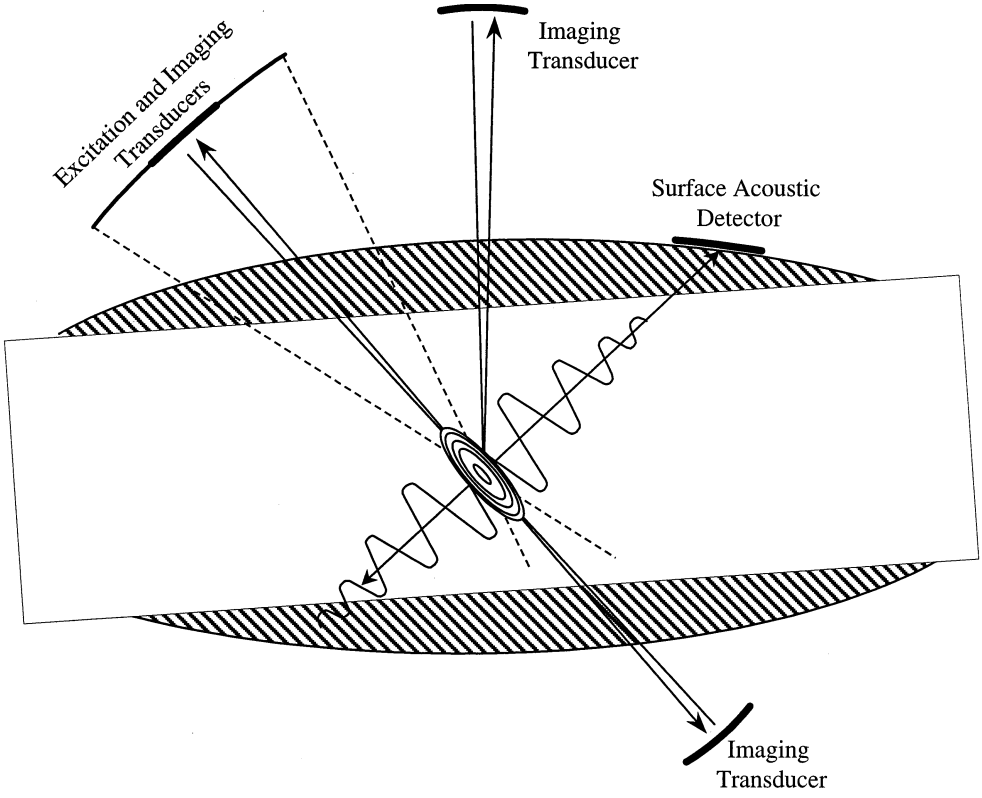

Fig. 2. Schematic presentation of shear wave elasticity imaging. A shear wave excitation transducer as well as various imaging transducers and detection sensors are shown. Other imaging modalities, such as magnetic resonance imaging, also can be used to detect shear waves.

Finally, any appropriate imaging technique capable of detecting internal motion can be used for detection of shear waves remotely induced by radiation force of focused ultrasound. Compared to other imaging modalities, ultrasonic and MRI systems have a major advantage for SWEI: both imaging systems can exploit signal phase for accurate motion estimation. The possibility of merging SWEI and ultrasonic imaging has been discussed previously (Sarvazyan et al. 1995c), and use of MRI technologies in SWEI is illustrated and discussed following.

THEORY

Mathematical model

This section presents further development of a theoretical model of remotely inducing shear oscillations in soft biological tissue by the radiation force of a focused ultrasound beam derived recently (Rudenko et al. 1996). Radiation force and induced shear oscillations can be derived from the well-known Khokhlov-Zabolotskaja-Kuznetsov (KZK) equation (Novikov et al. 1987; Rudenko et al. 1990, 1996):

$$\frac{\partial}{\partial \tau}\left[\frac{\partial p}{\partial x}-\frac{\varepsilon}{c^3\rho}\,p\,\frac{\partial p}{\partial \tau}-\frac{b}{2c^3\rho}\,\frac{\partial^2 p}{\partial \tau^2}\right]=\frac{c}{2}\,\Delta_{\perp}p, \qquad (1)$$

where p is acoustic pressure, x is the axis of the cylindrical coordinate coinciding with the axis of the acoustic beam, ε is the parameter of nonlinearity, ρ is the density of medium, c is the speed of sound, $\tau = t - x/c$ is time in the moving coordinate system commonly used in nonlinear acoustics (Rudenko and Soluyan 1977), and $\Delta_{\perp}$ is the Laplacian operator acting on the transverse coordinate r.

The solution of this KZK eqn (1) can be used to find the field of radiation forces (Rudenko et al. 1990, 1996):

$$F_x=\frac{b}{c^3\rho}\overline{\left(\frac{\partial p}{\partial \tau}\right)^2}, \qquad (2)$$

where F_x is the component of the radiation force acting along the beam direction, b is the effective dissipation, and the overbar denotes averaging over the ultrasound wave period. This force induces low-frequency shear oscillations in the surrounding tissue in the same x-direction. The oscillations are described by the following equation:

$$\frac{\partial^2 s_x}{\partial t^2}-\left(c_t^2+v\,\frac{\partial}{\partial t}\right)\Delta_{\perp}s_x=F_x, \qquad (3)$$

where $c_t = \sqrt{\mu/\rho}$ is the speed of the shear waves propagation, μ is the shear elastic modulus, $\nu = \eta/\rho$ is the kinematic shear viscosity, and s_x is a component of the displacement vector along the x direction. Equation (3) also can be derived from general equations of the dynamic theory of elasticity (Landau and Liftshitz 1965), assuming that the shear elastic modulus μ is small compared to the compression modulus. Moreover, the spatial variations of s_x should be different depending on the direction: changes of the displacement profile in a radial direction occur faster than in axial. This assumption corresponds well to both conditions of shear waves excitation (Fig. 2) and known approximations (Rudenko and Soluyan 1977) used to derive KZK type eqn (1). Note that, in the absence of shear elasticity ($\mu = 0$), eqns. (2) and (3) coincide with the known equations used to calculate nonstationary Eckart acoustic wind (Rudenko and Soluyan 1977). Therefore, the complete mathematical model of remote shear waves excitation induced by modulated ultrasound in viscoelastic waterlike materials is described by eqns. (1) through (3).

It is necessary to solve the wave eqn (1) with the following boundary condition:

$$p(x = 0,r,t) = p_0\Phi\left(\frac{r^2}{a^2}\right)\varphi(\Omega t)\sin\omega\left(t + \frac{r^2}{2cd}\right). \quad (4)$$

Here, p_0 is acoustic pressure on the beam axis, which is coincident with the x-axis of the cylindrical coordinate system, Ω is the modulation frequency, ω is the ultrasound frequency, c is the speed of sound, and d and a are, respectively, the curvature radius and the aperture of the single element excitation transducer. Note that parameter d also represents the geometric focus of the transducer. The functions μ and ν describe the transverse profile of the beam and the envelope of modulation, respectively.

The solution of a linear problem for a focused beam with initial Gaussian profile $\Phi = \exp(-r^2/a^2)$ has a simple form (Vinogradova et al. 1990):

$$p = \frac{p_0}{f(x)}\,\varphi(\Omega t)\exp\left(-\alpha x - \frac{r^2}{a^2 f^2(x)}\right) \times \sin(\omega t + \phi(x, r)), \quad (5)$$

where α is an attenuation coefficient,

$$\alpha = \frac{b\omega^2}{2c^3\rho}, \quad (6)$$

and function $f(x)$ simultaneously describes changes in both axial wave amplitude and Gaussian beam width,

$$f(x) = \sqrt{\left(1 - \frac{x}{d}\right)^2 + \frac{x^2}{x_d^2}}, \qquad x_d = \frac{\omega a^2}{2c}, \quad (7)$$

where x_d is the characteristic diffraction length (Rayleigh distance). Function $\phi(x,r)$ in eqn (5) describes changes in the position and the curvature of the phase front during focusing,

$$\phi(x,r) = \arctan\frac{x/x_d}{1 - x/d} + \pi\mathrm{H}(x - d) - \frac{r^2}{a^2}x_d\frac{d}{dx}[\ln f(x)], \quad (8)$$

where H is a Heaviside step function.

Nonlinear effects

Various asymptotic solutions of a nonlinear problem describing the focusing of intensive beams are known (Hamilton et al. 1997; Rudenko 1995). These solutions are not presented in the article, but will be used for calculation of wave characteristics such as power and intensity of the beam, and radiation force.

In linear approximation, these characteristics are calculated using simple analytic solutions such as eqn (5). Radiation force can be found by substituting eqn (5) into eqn (2):

$$F_x = \alpha\, c^2\left(\frac{p_0}{c^2\rho}\right)^2 \frac{\varphi^2(\Omega t)}{f^2(x)}\exp\left(-2\alpha\, x - \frac{2r^2}{a^2 f^2(x)}\right). \quad (9)$$

For weak diffraction, i.e., $D = d/X_d << 1$, the radiation force [eqn (9)] has a sharp peak near the geometric focus $x = d$. The intensity distribution I follows the spatial distribution of radiation force, and the full power ∂ (integral of intensity over the beam cross-section) monotonically decreases with increase of the distance x due to dissipative losses of the wave energy:

$$I = \frac{\rho c}{2\alpha}F_x, \qquad M = \frac{\pi a^2 p_0}{4\rho c}\,\varphi^2(\Omega t)\exp(-2\alpha x). \quad (10)$$

The structure of the radiation force field for both weak and high-intensity beams, requiring the consideration of nonlinear effects, was investigated previously (Rudenko et al. 1996). Using the same approach, more detailed calculations have been performed. The solid lines in Fig. 3 show the solution of a linear problem, i.e., eqns (9) and (10). The full power (a), intensity (b), and radiation force (c) on the beam axis $r = 0$ are shown as a function of the normalized distance x/d.

For better explanation of behavior of these and others curves in shown Fig. 3, the following three dimensionless parameters characterizing acoustic nonlin-

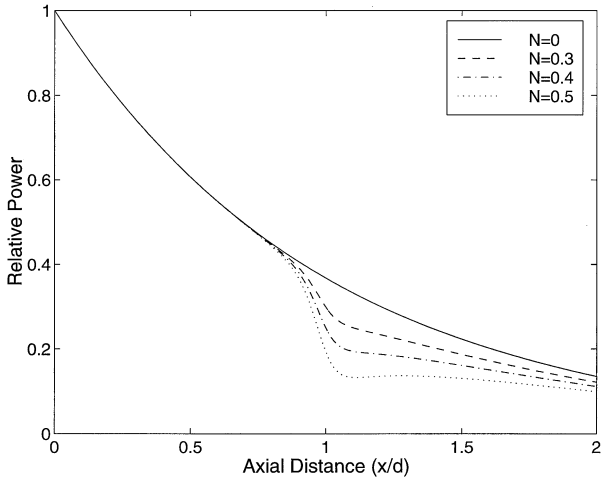

(a)

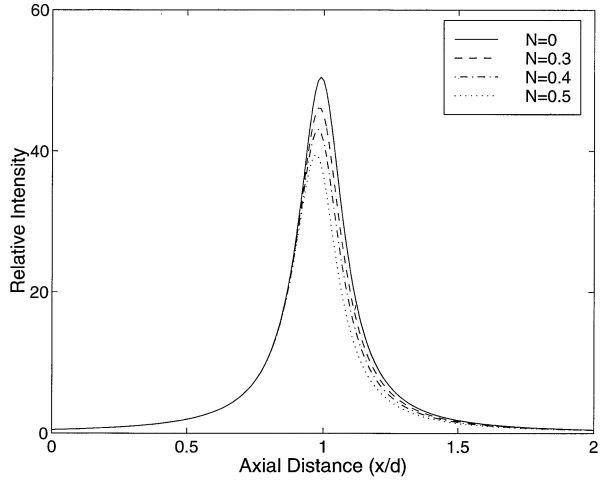

(b)

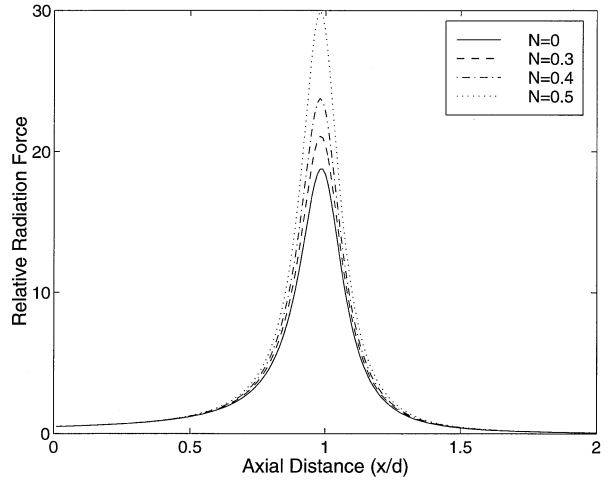

(c)

earity (N), linear energy dissipation (G), and diffraction (D) should be introduced:

$$N = \frac{d}{x_s}, \qquad G = \frac{d}{x_a}, \qquad D = \frac{d}{x_d}. \tag{11}$$

Here, d is the focal length of the transducer, x_d is the diffraction length [eqn (7)], x_a is the dissipative length (i.e., the distance where the wave amplitude is reduced by 1/e), and x_s is the nonlinear length, i.e., the distance where the shock wave is formed from originally plane harmonic waves (Rudenko and Soluyan 1977). If the values N, G, and D are small compared to unity, the corresponding processes (nonlinearity, absorption, or diffraction, respectively) are not pronounced over the distance d from ultrasound transducer to the focal zone. With an increase of N, G, and D, the influence of the corresponding process will increase.

In Fig. 3, the following parameters were used: $D = 0.1$, $G = 1$, i.e., the focal length is ten times smaller than diffraction length but comparable to the dissipative length. It can be seen clearly from Fig. 3a that, with increasing of nonlinearity N, the power, exponentially decreasing with distance due to the linear dissipative losses [eqn (10)] in the prefocal zone, suddenly further decreases in the focal region where nonlinear effects are more pronounced. Increase of nonlinearity N emphasizes this effect.

The maximum of intensity (Fig. 3b) appears near the focal region $x = d$. Additional nonlinear absorption, related to generation of higher frequency harmonics, reduces the intensity in the focal zone. Conversely, the radiation force magnitude (Fig. 3c) increases whereas the width of a radiation force curve (i.e., the area of the force localization) decreases. Clearly, the nonlinear effects may be useful for localized shear wave excitation.

However, such conclusions are only valid for moderate nonlinear effects. When the wave intensity is much higher ($N >> 1$), the initial sinusoidal ultrasound wave transforms into sawtoothlike wave before it reaches the focal zone. Within each period of the sawtoothlike wave, a narrow shock front can be formed and strong nonlinear absorption occurs. This absorption does not depend on linear dissipative properties of tissue determined by viscosity, thermal conductivity, relaxation, etc. (Rudenko 1995).

Fig. 3. Nonlinear enhancements of radiation force contrasted with the linear case. The ultrasound field characteristics: (a) power, (b) intensity, and (c) radiation force are plotted as a function of axial distance for linear (N=0) and nonlinear (N=0.3, 0.4, and 0.5) regimes.

Nonlinear losses of wave energy occur along the entire path from the transducer to the focus. These losses certainly are not useful for producing a localized peak of the radiation pressure in the vicinity of the focal region. Ideally, the wave energy should be transmitted in the prefocal zone without nonlinear losses, and nonlinear losses should appear only near the focus, so that the nonlinear enhancement of the radiation force would be localized in a small tissue volume.

It may look simple to implement this ideal localized excitation of the shear waves. Indeed, the intensity of the initial wave must be chosen so that nonlinear wave profile distortions accumulated along the wave propagation distance would result in a shock front formation precisely in the focus, whereas the wave profile remains smooth within the prefocal region. However, this is difficult to achieve, because diffraction leads to frequency-dependent phase shifts [eqn (8)]. The overall phase shift at the focal zone is approximately π, where a significant portion of this shift occurs within the $D{\cdot}d$ region. The frequency-dependent phase [eqn (8)] implies that, in the focal region, harmonics propagate with different speeds. As a result, the shock front in the focal region is less emphasized, reducing the expected nonlinear effect in enhancement of localized generation of radiation force.

Figure 4a illustrates such an effect. The initial wave profile over one period has a sawtooth form. Both linear and nonlinear absorption occur during wave propagation, and the wave amplitude is monotonically decreased. Near the focus, the phase shifts due to diffraction transform the wave front so that, near and beyond the focal region, linear dissipation is dominant. Consequently, the advantage of nonlinear mode in the enhancement of the radiation force disappears. This undesired phase shift effect can be compensated, however, if a driving signal consisting of weighted harmonics (i.e., harmonics with certain amplitude and phase values) can be generated. The amplitude and phase shift for each harmonic can be chosen so that the nonlinearity, diffraction, and dissipation will transform the initial wave into a shock wave near the focal region. In addition, only linear and, therefore, not significant losses will take place along the prefocal distance, and the maximum transfer of ultrasonic energy into radiation force will occur at the focus.

To find the wave profile corresponding to maximum radiation force generation at the focal region, the nonlinear inverse problem needs to be analyzed. Mathematical methods to solve this inverse problem accounting for nonlinear effects are beyond the scope of this article. In Fig. 4b, however, one example of solving this inverse problem and designing an optimal wave profile is given. To enhance the radiation force in the focal area, the initial profile of one wave period should have a narrow positive and a broad negative acoustic pressure profile.

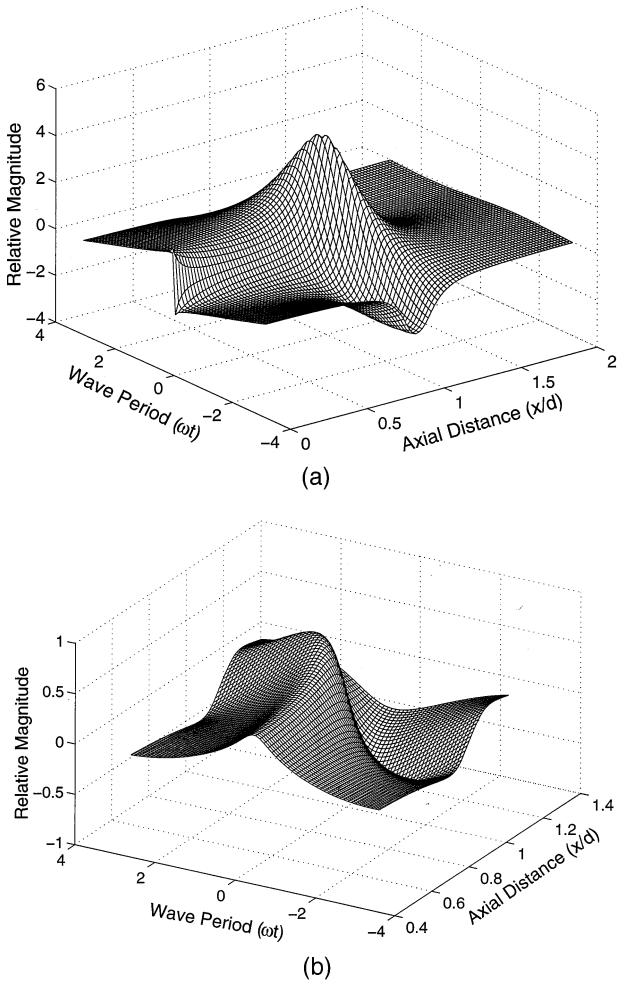

Fig. 4. (a) Transformation of the waveform for a focused ultrasonic field. The initial wave profile has a sawtooth form. (b) Illustration of the optimal waveform profile for shear wave elasticity imaging based on the inverse problem solution of nonlinear acoustics. The sawtooth wave profile is produced in the focal zone of the focused ultrasonic field.

The geometric convergence, absorption, nonlinearity, and phase shifts due to diffraction transform this wave profile into a sawtoothlike wave near the focus, greatly enhancing the nonlinear absorption in the focus.

Therefore, properly accounting for the ultrasonic properties of tissue, the nonlinear effects can enhance the amplitude and localization of the radiation force in the focal region.

Generation of shear wave and evaluation of shear properties of tissues

Radiation force will induce shear oscillations in tissue as described in eqn (3). Our goal here is to derive an analytic solution to eqn (3), useful for analysis and understanding of physical properties of the shear wave genera-

tion. This derivation of an analytic solution is only possible for linear absorption of ultrasound. After obtaining a description of the linear approximation, one can further estimate the possible contribution of nonlinearity to the effect.

To solve shear wave eqn (3) with radiation force eqn (9), the Hankel transformation can be used:

$$s_x(r,t) = \int_0^\infty \tilde{s}(\beta, t) J_0(\beta r) \beta d\beta, \qquad (12)$$

where J_0 is the Bessel function of the first kind, zeroth order. The time behavior of the Hankel transform $\tilde{s}$ is described by the equation of forced and decayed oscillations:

$$\frac{d^2\tilde{s}}{dt^2} + \beta^2 \nu \frac{d\tilde{s}}{dt} + \beta^2 c_t^2 \tilde{s} = \frac{\alpha a^2 I_0}{2c\rho} e^{-2\alpha x} e^{-\frac{a^2 f^2}{8}\beta^2} \varphi^2(\Omega t), \quad (13)$$

where $I_0 = {p_0}^2/(2\rho c)$ is the intensity of the initial ultrasound wave on the beam axis. The displacement s_x can be found by solving the ordinary differential equation for $\tilde{s}$ and using the Hankel transform eqn (12):

$$s_x = \frac{\alpha a^2 I_0}{2c\rho} e^{-2\alpha x} \int_0^\infty \frac{e^{-\frac{a^2 f^2}{8}\beta^2} J_0(\beta r)\beta d\beta}{\sqrt{\beta^2 c_t^2 - \beta^4 \nu^2/4}} \int_0^t \varphi^2(\Omega t') e^{-\frac{\beta^2 \nu}{2}(t-t')} \times \sin((t-t')\sqrt{\beta^2 c^2 - \beta^4 \nu^2/4}) dt'. \quad (14)$$

This eqn (14) describes the displacement $s_x(x,r)$ at any time. It also is assumed here that the envelope signal $\varphi(\Omega t)$ starts at $t = 0$.

We will further consider two important cases: periodic and pulsing modulation. When the ultrasound signal is modulated so that $\varphi^2 = \sin(\Omega t)$, it is convenient to present the displacement s_x in the form:

$$s_x = \frac{\alpha a^2 I_0}{2c\rho} e^{-2\alpha x} \int_0^\infty \frac{e^{-\frac{a^2 f^2}{8}\beta^2} J_0(\beta r)\beta}{\sqrt{(\beta^2 c_t^2 - \Omega^2)^2 + (\Omega\beta^2\nu)^2}} \times \sin\left(\Omega t - \arctan\frac{\Omega\beta^2\nu}{\beta^2 c_t^2 - \Omega^2}\right) d\beta. \quad (15)$$

Spatial distribution of axial displacement magnitude $s_x(x,r)$ at some arbitrarily chosen time is shown in Fig. 5. This figure presents the displacement s_x [eqn (15)] obtained for periodic low-frequency modulation of an ultrasonic beam and the following parameters of the transducer/tissue: $\frac{\omega}{2\pi} = 3$ MHz, $\frac{\Omega}{2\pi} = 1$ kHz, $a = 0.01$ m, $d = 0.05$ m, $I_0 = 10$ W/cm^2, $\rho = 1000$ kg/m^3, $c = 1500$ m/s, $c_t = 3$ m/s, and attenuation α was chosen similar to liver. Clearly, the absolute maximum of the displacement s_x is near the geometric focus $x = d$ on the axis of ultrasound beam. Neighboring local minima and maxima are about half of a wavelength from each other. Such structure is a characteristic of the near field where wave propagation has not yet stabilized. The estimates show that, due to high attenuation of shear waves in the tissue, the wave typically will decay before it can reach the far-field region. Therefore, knowledge of the displacement pattern near the beam axis (see Fig. 5) becomes very important. Figure 5 shows only axial displacement, and the radial displacements can be found from the equation of continuity, div $\vec{s} = 0$. It should be noted here, however, that radial displacement is an order of magnitude smaller than axial displacement.

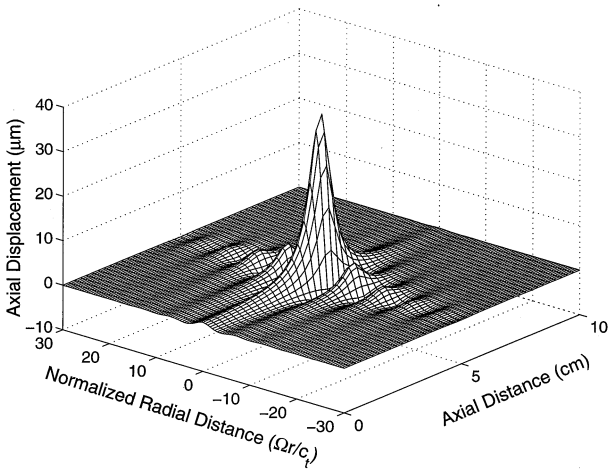

Fig. 5. Typical distribution of the axial (i.e., shear) displacement induced by radiation force of focused ultrasound.

Shear waves also can be induced in tissue using pulsing ultrasonic modulation. For ultrasonic pulse modulation, eqn (14) can be written in the form:

$$s_x = \int_0^t \varphi^2(\Omega t') G(x, r, t-t') dt', \qquad (16)$$

where $G(t)$ is Green's function:

$$G(t) = G_0 c_t \int_0^\infty e^{-\frac{\beta^2}{8}(a^2 f^2 + 4\nu t)} \frac{\sin(t\sqrt{\beta^2 c_t^2 - \beta^4 \nu^2/4})}{\sqrt{\beta^2 c_t^2 - \beta^4 \nu^2/4}} \times J_0(\beta r)\beta d\beta, \quad (17)$$

$$G_0 = \frac{\alpha a^2 I_0}{2cc_t\rho} e^{-2\alpha x}. \qquad (18)$$

It is impossible analytically to evaluate Green's function in eqn (17). However, using two realistic assumptions, the problem can be simplified and the integral eqn (17) can be calculated analytically. The first simplification is based on evaluation of physical parameters in eqn (17). For most soft tissue types, the viscosity does not exceed 10 Pa·s, shear velocity lies in the range 0.5–50 m/s, and the typical time scale for SWEI experiment is about 1 ms. In this case, the second negative term under square roots in eqn (17) can be neglected. Physically, it means that shear vibration is not damped entirely and has the decaying oscillation form [see eqn (13)], i.e., the shear wave can propagate through a distance of several wavelengths. The second simplification is based on mathematical modeling of bell-like Gaussian function of β by an exponential one. The transverse profile of the ultrasonic beam and its Fourier transformation with such an assumption have the form:

$$\Phi = \frac{af}{(r^2 + a^2f^2)^{3/2}}, \tilde{\Phi} = e^{-af\beta}. \tag{19}$$

Under these two conditions, the Green's function takes the form:

$$\frac{G}{G_0} = \frac{1}{\sqrt{2}}\left[\frac{\sqrt{H_1^2 + H_2^2} - H_1}{H_1^2 + H_2^2}\right]^{1/2}, \tag{20}$$

where

$$H_1 = a^2f^2 + 4vt - c_t^2t^2 + r^2,$$

$$H_2 = 2c_t t\sqrt{a^2f^2 + 4vt}. \tag{21}$$

For the modulation pulse with duration shorter than the time required for shear wave to pass across the beam, eqns (16) and (20) in focus $r = 0$, $x = d$ takes a simple form:

$$s_x = \frac{\sqrt{\pi}}{2}\frac{\alpha a^2 I_0}{c\sqrt{\rho\mu}} e^{-2\alpha d}\left(\frac{t_0}{aD}\right) \times \frac{\left(\frac{\sqrt{\mu/\rho}}{aD}\right)t}{1 + \frac{4vt}{(aD)^2} + \left(\frac{\sqrt{\mu/\rho}}{aD}\right)^2 t^2}, \tag{22}$$

where t_0 is the duration of modulating pulse. The analysis of spatial and temporal behaviors of shear displacement is presented in Fig. 6, where temporal behavior of axial displacement was computed for a 100-μs duration

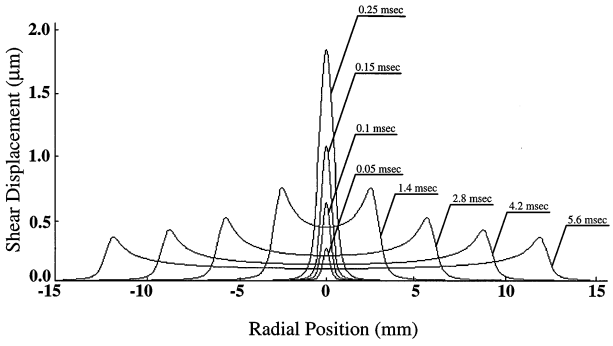

Fig. 6. Temporal and spatial behavior of axial shear displacement along the radial direction at the focal point of the transducer.

rectangular modulating pulse acting on the elastic media with shear wave speed set to 2.1 m/s. The displacement increases initially in time, after the exciting ultrasonic pulse arrives at the focal area. Reaching a maximum at $t_{max} = aD/c_t$, the displacement starts to decay, due to the formation of a cylindrical wave in the form of a doughnut propagating away from the axis. As it follows from eqns (16) and (17), the distance between the wave front and axis of the beam linearly increases as $t{\cdot}c_t$, and the wave magnitude decreases due to wave divergency. The decrease of the magnitude will be more pronounced in viscous media, and the front of the shear wave will become much wider. Note that similar behavior is demonstrated in Fig. 13b, which was calculated for specific acoustic and material parameters in nuclear magnetic resonance detection of shear wave as described in detail in the next section.

Because the region of localization of the radiation force is much larger in the axial than in the radial direction, it is the cylindrical wave that is generated by the acoustic pulse. In Fig. 7, a typical three-dimensional (3D) plot (a) and two-dimensional (2D) topographic contour lines (b) for the radiation force induced by ultrasound in liverlike material are shown. The beam from a 3-MHz focused transducer first propagated through the 3-cm layer of water, and then it is focused in tissue 2 cm from the water–tissue boundary. Obviously, oscillation of an elongated object such as the focal region will generate waves that can be approximated by cylindrical waves.

From Fig. 6, various approaches of measuring the tissue viscoelastic properties can be suggested. The first approach is based on the measurement of the shear displacement in the focal region. Measurement in the single focal point has the advantage that shear displacement is largest at this point. In addition, displacement estimation at one single point can be simple and more convenient for technical implementation. As discussed

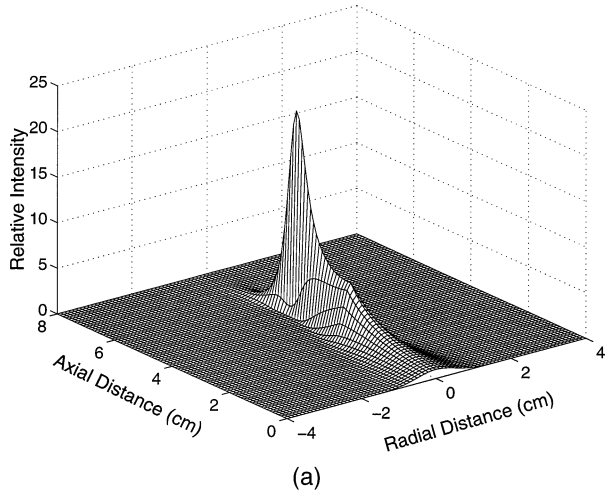

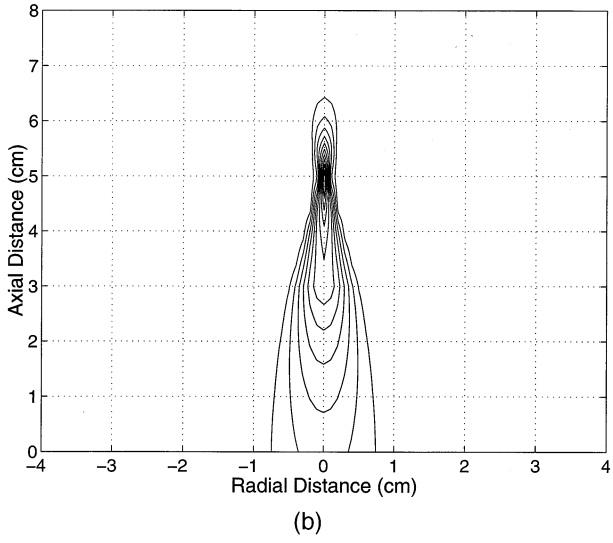

Fig. 7. Radiation force distribution of the focused ultrasound beam. (a) Three-dimensional plot; (b) two-dimensional topographic contour lines.

previously, temporal characteristics of shear displacement in the focal region contain information about both shear elasticity and dynamic shear viscosity of the tissue, and two different methods of assessing shear elasticity and viscosity can be used. First, measurements of the time required for the displacement to reach maximum at the focal point can be used for shear modulus estimation: $\mu = \rho(aD/t_{max})^2$, and the rate of the displacement decrease depends on the tissue viscosity, as shown in Fig. 8. The time $\Delta\tau$ needed to decrease the displacement to the certain chosen level (the level in Fig. 8 was chosen as -3 dB) can be used to evaluate the dynamic shear viscosity of the tissue. Second, tissue shear elasticity also can be calculated from the maximum axial displacement in the focal point, because the maximum displacement is

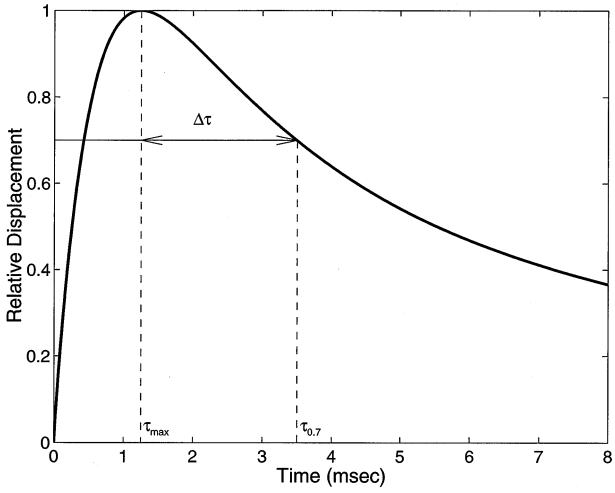

Fig. 8. Temporal behavior of the normalized shear displacement at the focal point of the transducer.

inversely proportional to the shear elasticity modulus. For example, the maximum displacement in brain tissue (having small shear elasticity modulus) will be larger than that in muscle. Therefore, it is possible to compare shear moduli of various tissues and to estimate their absolute values by measuring shear displacement s_x in the focal point in standardized controlled conditions.

Another approach of shear modulus estimation is based on the measurement of shear wave propagation parameters and changes in wave front position. Figure 9 shows profiles of the shear wave propagating radially through a region of tissue containing a small 2-mm wide hard inclusion. The wavefront was calculated for different time intervals after the generation of the wave. The same parameters as those used for Fig. 6 were used for

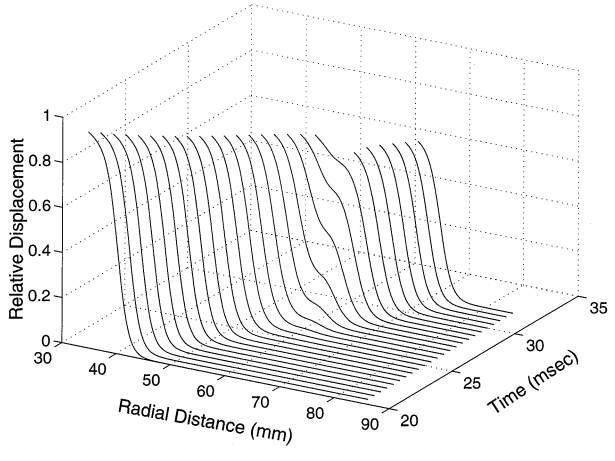

Fig. 9. Shear wave front propagation in tissue with a hard 2-mm inclusion.

the calculation. Estimation of the time needed for the wavefront to propagate from one point to another, and the distance between these two points, provide the shear wave speed c_t and, consequently, shear modulus μ. Attenuation of the propagating wave depends partially on the shear viscosity of the tissue.

To conclude this section, it is necessary to emphasize once again that we tried to derive results in a simple and clear analytic form. Such an approach offers the possibility for better understanding of the principles of the SWEI method. However, analytic results can be obtained in the special case that the problem is linear, but the linear solution qualitatively can describe only the most general aspects of shear dynamics and can predict the basic characteristics of the process without the desired precision. In reality, the behavior of focused ultrasound in the focal area is significantly nonlinear at peak intensities of 1 kW/cm^2, typical for conventional medical imaging. Some of the nonlinear phenomena principles for shear wave generation by focused ultrasound were discussed, based on the results of preceding work (Rudenko et al. 1996). It is not necessary to describe nonlinear theory here in more detail because it is too complex and quantitative results can be obtained mainly by numerical methods. However, in developing SWEI devices, it will be necessary to consider a numerical solution to the nonlinear problem eqns (1) through (3), because the nonlinear regime has advantage over the linear one. It gives the possibility to enhance typical shear displacement from 10^1 to 10^2 μm and makes it more easily detectable.

In addition to nonlinearity, an advanced theory of SWEI also must take into account the specific dissipative properties of a given kind of tissue to be examined. In such mathematical model, the KZK eqn (1) must be replaced by a nonlinear integro-differential equation:

$$\frac{\partial}{\partial t}\left[\frac{\partial p}{\partial \tau} - \frac{\varepsilon}{c^3\rho}\, p\, \frac{\partial p}{\partial \tau} - \gamma \frac{\partial^2}{\partial \tau^2} \times \int_0^\infty K(\xi)\, p(\tau,\, \tau - \xi)\, d\xi\right] = \frac{c}{2}\, \Delta_\perp p, \quad (23)$$

The kernel K inside the integral term in eqn (23) can be calculated for arbitrary dependences of dispersive and dissipative characteristics of the medium upon the frequency, using a standard procedure described by Vinogradova et al. (1990). Equation (23) was first proposed by Rudenko et al. (1974). In the case when the time delay in integral of eqn (23) can be neglected and assuming that

$$\gamma K(\xi) = \frac{b}{2c^3\rho}\, \delta(\xi), \quad (24)$$

where δ is the Dirac delta-function, then eqn (23) is transformed into the well-known KZK eqn (1). In biological tissues, the frequency dependence of the absorption coefficient usually has a form $\alpha \sim \omega^{1+\chi}$, where $0 < \kappa < 1$, and the corresponding kernel in eqn (23) can be written as:

$$K = \xi^{-\kappa} \quad (25)$$

Kernel eqn (25) describes the "memory" of medium decaying in time according to power law. The form of eqn (25) is a result of superposition of multiple internal processes in tissue having the nature of molecular relaxation. The form of eqn (25) is the simplest but not unique among all possible kernels, which can describe correctly the ultrasonic absorption in MHz frequency region.

EXPERIMENTAL STUDIES

Experimental studies are presented in this article to validate the SWEI method described here. Description of these experiments and results are given below.

Optical detection of shear waves

The first set of experiments, described in detail elsewhere (Andreev et al. 1996, 1997a), was designed to estimate the magnitude of the shear wave induced by focused ultrasound and to determine the requirements for an imaging system capable of detecting such motion in the tissue. The results of this study are discussed here to confirm the theoretical findings described in this article. A schematic diagram of the experimental system is illustrated in Fig. 10a. Briefly, the experiments were performed on a rectangular ($20 \times 20 \times 23$ mm^3) phantom made of rubberlike optically transparent material. Independent measurements of the density and shear elasticity modulus of this material yielded 0.98 g/cm^3 and 4600 Pa, respectively. Consequently, these measurements lead to a shear wave speed of 2.17 m/s. The measured absorption coefficient for this material was 0.5 dB/cm at 0.96 MHz and is well within the range of that for soft tissues. During phantom preparation, small (60–100 μm in diameter) particles were embedded in the central plane of the phantom. The phantom, attached to a 3D positioning system capable of producing micrometer scale displacements, was positioned in the water tank so that its geometric center coincided with the focal zone of an ultrasound transducer. The central plane of the phantom was positioned perpendicular to the surface of the transducer. The tank was filled with water to provide an acoustic coupling between the transducer and the phantom. Two

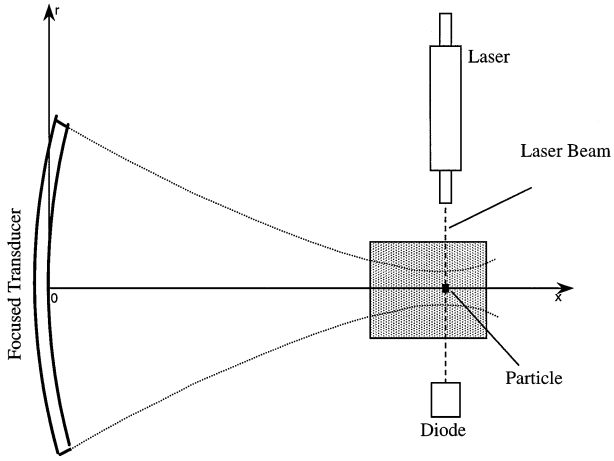

Fig. 10. Schematic view of the optical experimental set-up.

transducers were used in the experiment: they were a 64-mm curvature radius transducer with maximum acoustic power of 30 W operating at 0.96-MHz central frequency, and a 70-mm curvature radius transducer with maximum acoustic power of 15 W operating at 1.8-MHz central frequency. The transducers were attached to a linear positioning system allowing accurate lateral movement of the transducer.

Shear waves were detected using a laser-based optical system. First, the laser beam was focused on one of the particles so that it blocked the beam, and no signal was received on the diode. Then the phantom was moved in the axial direction (i.e., the direction of ultrasound propagation in the focus), and changes in the signal from the diode were recorded as a function of axial motion. The obtained dependence served as a calibration curve to determine the displacement of the particle due to ultrasonically induced shear waves in the media. The described laser-based system was capable of motion estimation in the range from 2–80 μm.

Measurements of shear wave propagation were based on estimation of the time necessary for the shear displacement to reach the maximum at each point along the radial coordinate. First, the transducer was placed so that the particle was in the focal zone of the transducer. Shear waves were induced in the media using a short pulse, and the signal on the diode corresponding to the particle motion was recorded on an oscilloscope. Then, the transducer was moved stepwise in the radial direction (i.e., perpendicular to the beam direction), the experiment was repeated, and the new signal from the diode was captured on the oscilloscope. Comparing two adjacent signals, the time of flight could be estimated from the change of the peak position between the two signals, and the magnitude of the shear displacement could be estimated from the magnitude of these peaks. These measurements were repeated for many points along the lateral coordinate, and the displacement and time of flight were estimated.

The magnitude of the displacement along the radial coordinate induced by a rectangular 0.1-ms ultrasonic pulse was measured. The maximum displacement at $r = 0$ is about 17 μm. Clearly, the displacement magnitude decreases as the shear wave propagates away from the focus. The time of flight of a shear pulse is linearly proportional to the distance of travel and the speed of shear waves was found to be 2 ± 0.2 m/s. This closely corresponds to the calculated shear wave speed of 2.17 m/s based on the independently measured density and shear modulus for this material.

The described experiment (Andreev et al. 1996, 1997a) was the first demonstration of the use of focused ultrasound to excite detectable shear waves. However, the optical method cannot be successfully used for biological tissues that strongly scatter light. More recently, this group of researchers (Andreev et al. 1997b) measured both shear displacement and shear wave velocity using remote detection by a probing ultrasonic pulse. The carrier frequency of exciting pulse was 2 MHz, and the intensity varied in the range from 10–30 W/cm^2. The rectangular envelope was 0.2 ms in duration. Induced shear motion was evaluated using a 10-μs long probing pulse at 3 MHz, by measuring the time delay for the pulse backscattered by moving inhomogeneity in the tissue. Maximum displacement in the propagating shear wave was > 10 μm and agrees with theoretical predictions.

Magnetic resonance imaging detection of shear waves

Several techniques have been used to detect bulk motion of materials using magnetic resonance imaging (Axel and Dougherty 1988; Decorps and Bourgeois 1991; Feinberg and Jakab 1990; Feinberg et al. 1985; Fowlkes et al. 1995; Manduca et al. 1996; Muthupillai et al. 1995; Plewes et al. 1995; Young et al. 1993; Zerhouni et al. 1988). The experiments presented here use motion sensitizing magnetic field gradient pulses. A pair of opposite polarity gradient pulses are applied in a particular direction (defined as x), which causes a phase shift in the magnetic resonance signal proportional to displacement in that direction. If there is no displacement, there is no net phase shift. Because the gradient has been applied along the x-axis, the method is sensitive to changes in position along the x-axis. The displacement at a given location is extracted from the magnetic resonance phase shift and sequence parameters. The time evolution of displacement, or propagation of a shear wave, is measured by recording the displacement as a function of the time between the acoustic pulse inducing the motion and the magnetic field gradient pulses.

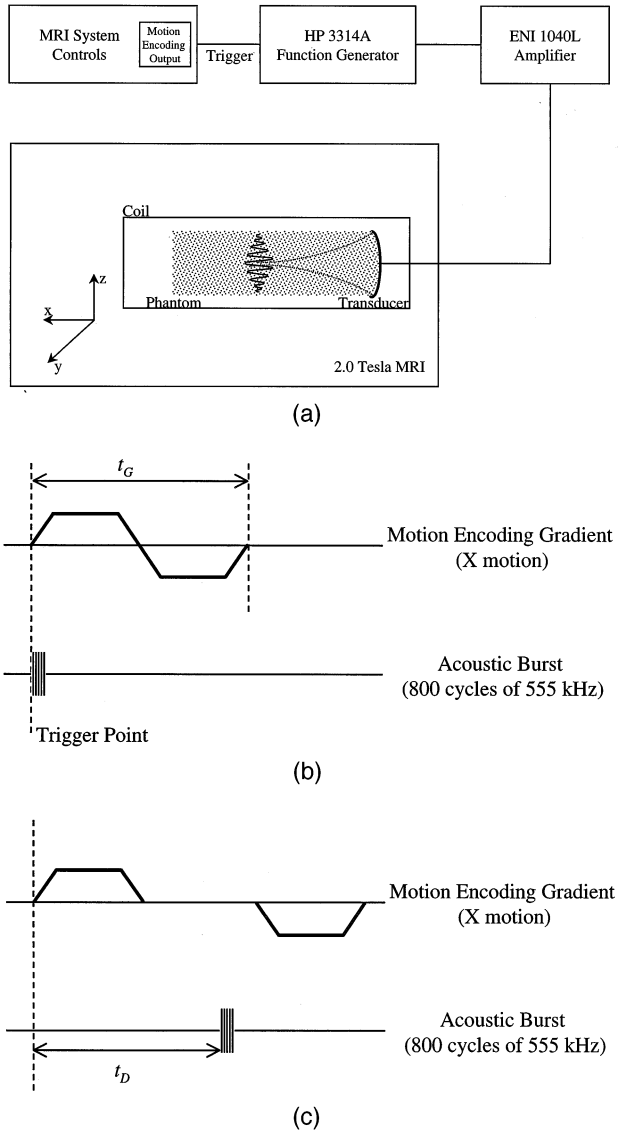

Fig. 11. Schematic view of the magnetic resonance imaging (MRI) experimental set-up. (a) Block diagram of the MRI system. (b) Diagram of the MRI motion-encoding gradient pulses shown with an acoustic pulse for the results of Fig. 12. t_G = Duration of gradient, which was set to 4.4 or 8.4 ms. (c) MRI pulse sequence for the results of Fig. 13a. t_D = delay time for the acoustic pulse after the positive gradient pulse is applied.

Two experiments were performed on a 2.0-T CSI Omega system (Fig. 11a) equipped with self-shielded gradients (General Electric, Fremont, CA, USA). In both experiments, the acoustic pulse of 3.6-ms duration at 555 kHz was generated by a 70-mm diameter PZT-4 transducer (Channel Industries, Santa Barbara, CA, USA) focused at a 100-mm depth within a cylinder of rubber (M-F Manufacturing Co., Fort Worth, TX, USA) measuring 280 mm in length and 100 mm in diameter. The shear wave speed for the rubber was 1.95 m/s as estimated from independent measurements of shear modulus and density for this material. A programmable TTL line from the Omega CSI triggered a waveform generator (model 395, Wavetek Inc., San Diego, CA, USA) whose output was amplified (model 1040L, ENI Corp., Rochester, NY, USA) and sent to the ultrasound transducer. The -3 dB depth of focus for this ultrasound transducer was $>$ 40 mm, providing a long axial excitation zone along the central axis for a 2D approximation of the shear wave propagation [see eqn (9)]. For each experiment, two data acquisitions were required, one with the acoustic pulse applied, and another with no acoustic energy (reference data set).

The first experiment provided an image of the displacement induced by the shear wave at two time points in its propagation. A conventional spin-echo pulse sequence was modified to include two pulsed magnetic field gradients with equal amplitude and duration, but opposite polarity. The gradients were applied in the x direction with a magnitude of 0.6 mT/cm. The displacement was measured in a plane parallel to the direction of the ultrasound propagation. Two data sets were acquired; one with the pulsed magnetic field gradient duration t_G at 4.4 ms and another at 8.4 ms. The timing of the acoustic pulse was held constant. Figure 11b is a diagram of the pulse sequence used for these experiments. This procedure produced images of shear displacement at two different times after the acoustic pulse was applied to the sample.

In the second experiment, a conventional spin-echo pulse sequence was modified to include two pulsed magnetic field gradients of opposite polarity applied in the x direction, 4.2 ms in duration, with a magnitude of 0.6 mT/cm. The TE of the spin-echo sequence was set to 50 ms, leaving an 18-ms window for the acoustic pulse. The timing and amplitude of the magnetic field gradients was held constant and the timing of the acoustic pulse t_D was controlled by the magnetic resonance pulse sequence. A one-dimensional column, 4 $\times$ 1 cm and normal to the direction of the ultrasound propagation, was selected by orthogonal slice selective 90° and 180° pulses. Figure 11c is a diagram of the pulse sequence used for these experiments. For each experiment, eight averages were acquired for each of 16 time points with 1-ms increments to measure the propagation of the shear wave.

The data sets were Fourier transformed and the phase angles between the referenced data set and data set with applied acoustic pulse were computed (Matlab, v 4.2, MathWorks Inc., Natick, MA, USA). The phase angle ϕ is a function of the gyromagnetic ratio of the nucleus γ, the magnitude and duration of the gradient $\nabla_x(t)$ and the trajectory of the volume element of the sample $x(t)$:

$$\phi = \gamma \int \nabla_x(t)\, x(t) dt. \tag{26}$$

Approximating the gradient waveform as a square wave with duration t and amplitude ∇_x and the trajectory as the average position $\tilde{x}$ results in a simplified expression for phase,

$$\phi = \gamma \nabla_x t \tilde{x}, \tag{27}$$

allowing calculation of the average position:

$$\tilde{x} = \frac{\phi}{\gamma \nabla_x t}. \tag{28}$$

Therefore, the shear displacement as a function of time can be estimated using eqn (28).

The distribution of the shear displacement in the longitudinal plane of the phantom at two different times is shown in Fig. 12. These images are displayed over an area 220 mm × 220 mm with the phantom positioned in the center, and the arrows indicate the location of the shear wave front. In these gray-scale images, full black represents no displacement, and full white represents the maximum motion along the ultrasound beam direction, i.e., shear displacement. Clearly, in the first image (Fig. 12a), the shear displacement is localized in the center of the phantom. Note that the region of localized displacement is elongated in the ultrasound beam direction, confirming the assumptions made previously to derive eqn (9). The shear displacement distribution at a later time (4 ms compared to the image in Fig. 12a) is shown in Fig. 12b. In this image, the shear wave already has propagated some distance away from the focal zone and appears as two symmetric bands on either side of the focal zone. Again, the regions of maximum shear displacement are elongated in the axial direction. Such a behavior of the shear wave is described by eqn (14) and closely corresponds to the simulation results presented in Fig. 6.

The results of the second experiment are shown in Fig. 13a. Here, the displacement in the *x* direction (direction of acoustic propagation and applied gradient) is plotted as a function of time and position along a line through the focus of the transducer and normal to the acoustic beam direction. The position of the peak displacement at each of the last eight time points was used to estimate the velocity of the wavefront and resulted in value of 2 m/s. This is in agreement with 1.95 m/s shear wave speed measured independently. The overall nature of these results for a homogeneous test object is very similar to measurements made by the optical techniques described previously (Andreev et al. 1996, 1997a).

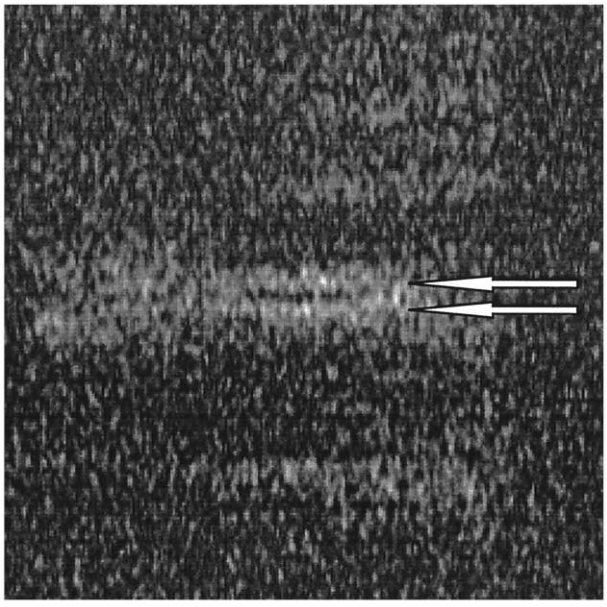

(a)

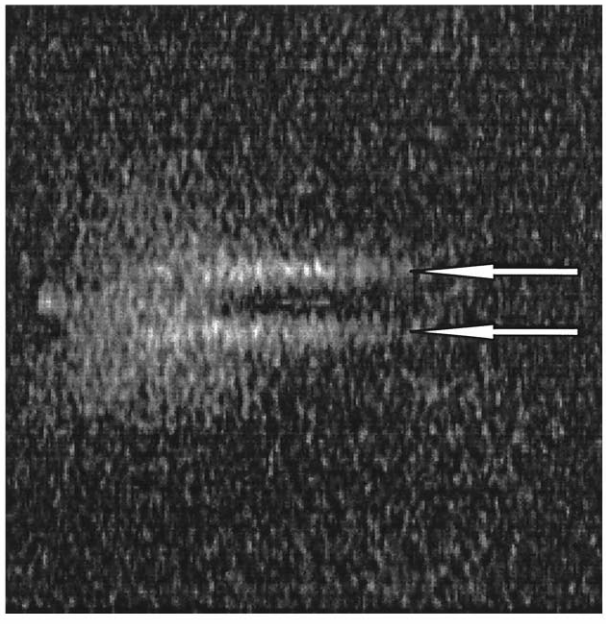

(b)

Fig. 12. Spatial distribution of the axial, shear displacement obtained for gradient times of (a) 4.4 ms and (b) 8.4 ms. Arrows indicate the position of the shear wave front.

Figure 13b shows simulated temporal behavior of the shear wave, as it is remotely induced and propagates within the tissue. The parameters of the ultrasound transducer and acoustic pulse from the experiment were used in this simulation, and data are presented in a similar form as in Fig. 13a. At the beginning, the shear displacement is induced by a radiation force of focused ultra-

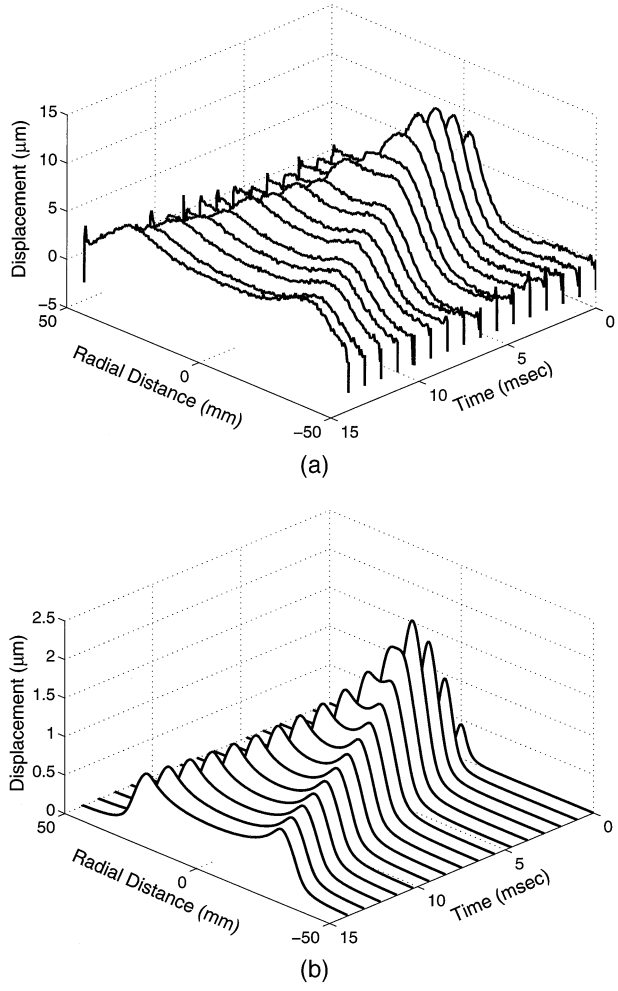

Fig. 13. Time evolution of the shear displacement along the radial position. (a) Measured; (b) simulated.

sound and continues to increase even after the acoustic pulse ends ($t = 0$). When the displacement reaches the maximum, the wave has already begun to diverge, propagating away from the focus and decaying in magnitude. At this time, the propagation of the wavefront is proportional to the shear wave speed in the medium.

The phenomenon of shear wave propagation can be better understood if both temporal and spatial characteristics are shown. The temporal behavior of the axial displacement s_x in the focal plane, i.e., in the plane near the geometric focus of the transducer and parallel to the beam axis, is presented in Fig. 14. A rectangular 100-μs duration acoustic pulse and shear wave speed $c_t = 2$ m/s were used in this simulation. Note the similarities in form between Figs. 12 and 14.

Initially, shear displacement magnitude along the beam axis increases with time (Fig. 14, $\tau = 0.3$, 0.6, and 1 ms). This increase continues due to inertia for some time after the acoustic pulse is terminated. Displacement reaches maximum at time τ_{max} needed for the shear wave to travel the distance equal to the radius a of the focal region: $\tau_{max} = aD/c_t$. Keeping in mind that $c_t = \sqrt{\mu/\rho}$, the shear modulus estimate, $\mu = \rho(aD/\tau_{max})^2$, can be obtained. After reaching the maximum, the displacement starts to decrease, due the absorption of the shear wave as well as the formation of diverging cylindrical wave propagating away from the axis (Fig. 14, $\tau = 2$–14 ms). At that stage, the distance between the wavefront and axis of the beam linearly increases as $c_t\ t$.

DISCUSSION AND DIRECTIONS OF FUTURE DEVELOPMENT

Elasticity imaging is evolving rapidly into a new diagnostic modality. In current approaches of tissue elasticity evaluation, an externally applied vibrator or static load induces a displacement, velocity, or strain pattern, which depends not only on the elasticity distribution, but also on global boundary conditions, i.e., the geometry of the object, types of external and internal forces, the mechanical constraint of the body, etc. SWEI is based on the analysis of temporal and spatial characteristics of remotely induced and highly localized shear strain. Consequently, local evaluation of viscoelastic properties is simplified greatly, because trivial boundary conditions can be assumed and an infinite medium model can be used to reconstruct tissue mechanical properties.

The core of the SWEI method is shear wave generation induced remotely by focused ultrasound radiation force. These waves then can be detected and analyzed to extract viscoelastic properties. In this article, an optical system and MRI were used to validate the theoretical model of SWEI, i.e., separate systems were used to create and monitor the shear wave. In ultrasound SWEI, however, ultrasound can be used both to produce a shear strain disturbance in the tissue and to monitor the evolution of shear strain as well as to image the internal tissue structures. Clearly, this method would require a transducer configuration that can control radiation force while simultaneously imaging the tissue and detecting small displacements induced by this force. Such multipurpose transducers would make the system more compact and, perhaps more importantly, provide independent feedback to monitor tissue changes.

Preliminary analysis of the range of required parameters for ultrasonic pulses to induce shear strain in tissue and of literature on damaging biological effects at these levels of ultrasonic exposure has been made. Figure 15 presents a summary of this analysis. Typical ultrasonic exposures for SWEI are significantly below the threshold of damaging effects of focused ultrasound, as shown in Fig. 15. The problem of SWEI safety is one of the key

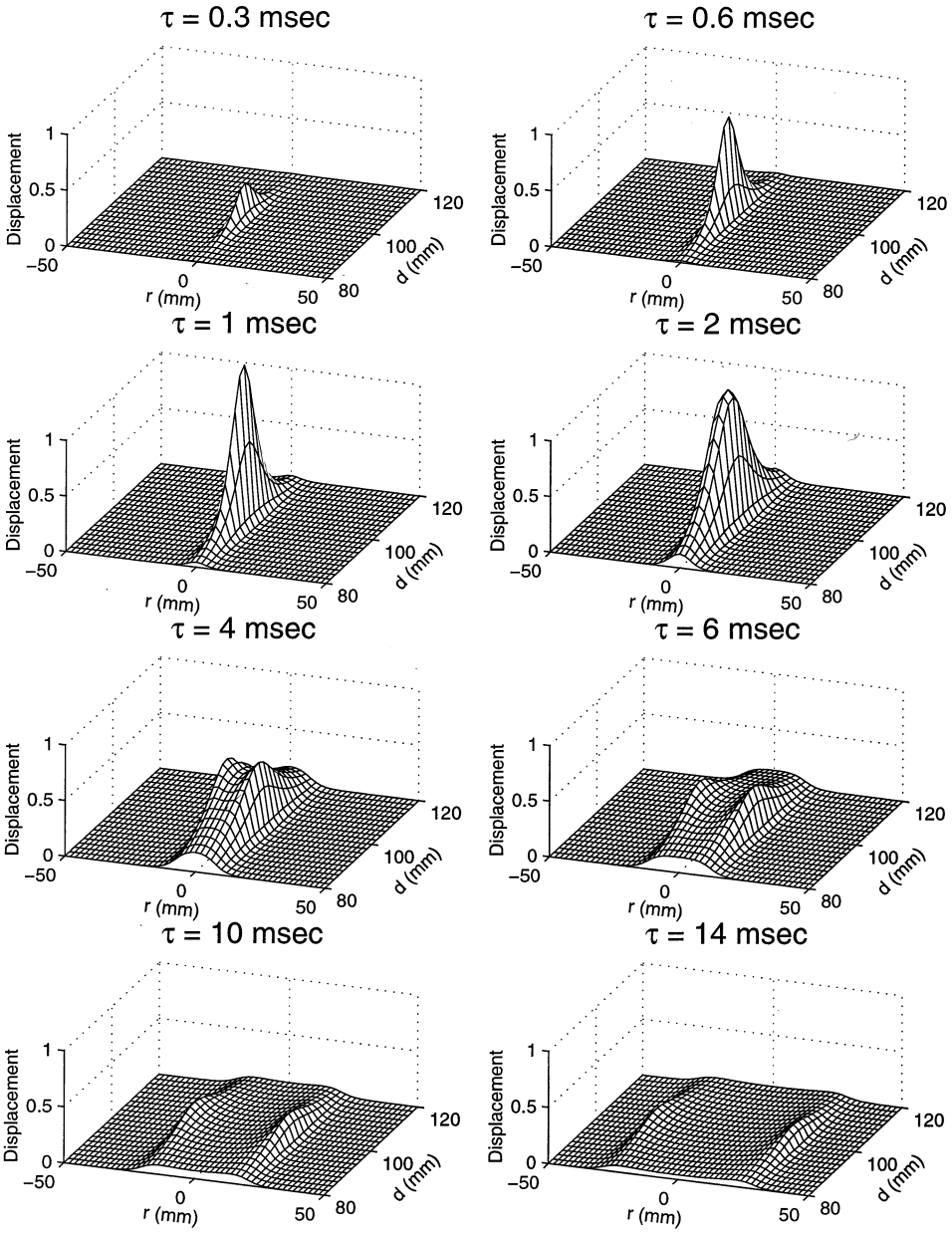

Fig. 14. Generation and propagation of the shear wave shown at different times after transmission of the acoustic pulse.

aspects of the feasibility of this approach and will be studied in more detail.

There are various possible implementations of ultrasound radiation pressure-based elasticity imaging. First, SWEI is a method for tissue characterization that can add a new quality to conventional ultrasonic imaging or MRI. Adding shear elasticity data ("palpation information") by, for example, superimposing color-coded elasticity data over an ultrasonic or magnetic resonance image, may enable better differentiation of tissues and enhances diagnosis.

SWEI is an independent imaging method in which shear modulus serves as the imaging parameter and the image is formed in terms of the spatial distribution of shear elasticity. SWEI might be used in various clinical applications such as detecting hard lumps in breast, diagnosing brain trauma and edema, evaluating tissue blood supply, and monitoring neuromuscular system healing. In addition, it is possible to form an image in terms of tissue shear viscosity. Shear viscosity is highly sensitive to tissue conditions, such as edema, muscle tone, etc. Currently, there are no other means to visualize shear viscosity of tissue, and such capability is one of the most unique features of SWEI.

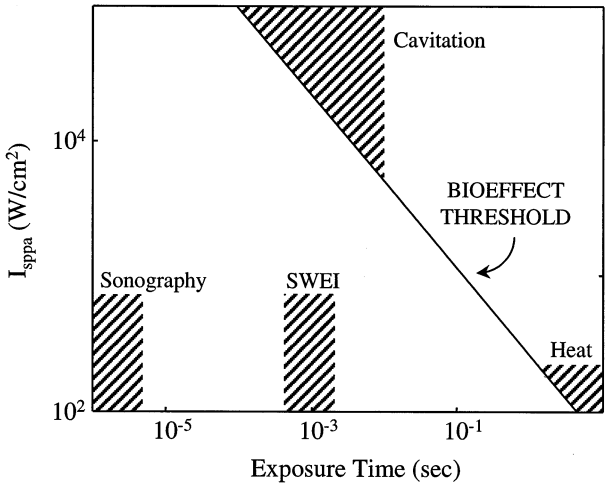

Fig. 15. Plot of intensity vs. exposure time showing the threshold for lesion production using focused ultrasound. The domains for thermal and cavitational mechanisms of damage are shown (ter Haar 1986). Shaded areas below the threshold line represent typical ranges of intensities and exposure times for pulse-echo imaging (Patton et al. 1994) and for shear wave elasticity (SWEI) imaging.

Other potential applications of SWEI are in the area of high-intensity ultrasound, where information derived from the real-time images is used to control dose and delivery of ultrasound energy. Indeed, SWEI can provide an excellent feedback and monitoring of tissue changes in ultrasonic hyperthermia, high-intensity focused ultrasound (HIFU) surgery, etc. It is even possible to design and build a multipurpose ultrasound transducer capable of visualization, hyperthermia/surgery, and monitoring functions.

Finally, there is a possibility to use SWEI for adaptive multiparametric imaging. The idea of such an approach is that the displayed parameter is composed of several independent variables, such as shear elasticity and viscosity obtained by SWEI, and other information available from a conventional imaging modality, such as bulk elasticity obtained from ultrasonic imaging, or spin-echo parameters available in MRI. Depending on the type of tissue analyzed, these measured variables are composed so that the objective of any particular medical diagnosis task optimally is fulfilled. This composition is designed to provide maximum separation of tissue types and conditions in the multidimensional space of variables. One of the numerous advantages of adaptive multiparametric imaging is that each parameter adds to the resolution, contrast, and sensitivity of the imaging system, and, consequently, its overall technical characteristics are superior to that of an imaging system based on any of these individual parameters separately. It is reasonable to assume that ultimately elasticity imaging will merge fully with conventional ultrasonic or nuclear magnetic imaging on the basis of adaptive multiparametric imaging.

In conclusion, a new approach to elasticity imaging—shear wave elasticity imaging—is presented in this article. Only theoretical and technical aspects of SWEI were considered. Many other issues, including the safety of SWEI, need to be considered before this method can be used for clinical studies. However, based on the preliminary results presented here, SWEI has the potential to become a valuable tool in clinical practice.

Acknowledgements—Helpful discussions with Matthew O'Donnell and Mark Lubinski from the University of Michigan, Valery Andreev and Oleg Sapozhnikov from Moscow State University, and Andrei Skovoroda from the Institute of Mathematical Problems in Biology (Russian Academy of Sciences) are gratefully acknowledged.

REFERENCES

Andreev V, Dmitriev V, Pischalnikov Y, et al. Excitation of shear waves by focused longitudinal wave. In: Wei RJ, ed. Proceedings of the 14th International Symposium on Nonlinear Acoustics. Nanjing: Nanjing University Press, 1996:457–462.

Andreev V, Dmitriev V, Pischalnikov Y, et al. Observation of shear waves excited by focused ultrasound in a rubber-like media. Acoustical Physics 1997a;43:123–128.

Andreev V, Dmitriev V, Rudenko O, Sarvazyan A. Remote generation of shear wave in soft tissue by pulsed radiation pressure. J Acoust Soc Am 1997b;102:3155.

Axel L, Dougherty L. Heart wall motion: Improved method of spatial modulation of magnetization for MR imaging. Radiology 1988; 169:59–63.

Cespedes I, Ophir J, Ponnekanti H, Maklad N. Elastography: Elasticity imaging using ultrasound with application to muscle and breast *in vivo*. Ultrason Imaging 1993;15:73–81.

Decorps M, Bourgeois D. Very slow flow imaging. Magn Reson Med 1991;19:270.

Duck FA. Physical properties of tissues. New York: Academic Press, 1990.

Emelianov SY, Skovoroda AR, Lubinski MA, O'Donnell M. Reconstructive elasticity imaging. In: Jones JP, ed. Acoustical Imaging 21. New York: Plenum Press, 1995:241–252.

Emelianov SY, Swanson SD, Fowlkes JB, Rudenko OV, Sarvazyan AP. Remote surrogate palpation: Shear wave elasticity imaging. Abstract of the 22nd Ultrasonic Imaging and Tissue Characterization Symposium. Ultrason Imaging 1997.

Feinberg DA, Jakab PD. Tissue perfusion in humans studied by Fourier velocity distribution, line scan, and echo-planar imaging. Magn Reson Med 1990;16:280–293.

Feinberg DA, Crooks LE, Sheldon P, et al. Magnetic resonance imaging the velocity vector components of fluid flow. Magn Reson Med 1985;2:555–566.

Fowlkes JB, Emelianov SY, Pipe JG, et al. Magnetic resonance imaging techniques for detection of elasticity variation. Med Phys 1995; 22:1771–1778.

Frizzell LA, Carstensen EL, Dyro JF. Shear properties of mammalian tissues at low megahertz frequencies. J Acoust Soc Am 1976;60: 1409–1411.

Goss SA, Johnson RL, Dunn F. Comprehensive compilation of empirical ultrasonic properties of mammalian tissues. J Acoust Soc Am 1978;64:423–457.

Hamilton MF, Khokhlova VA, Rudenko OV. Analytical method for describing the paraxial region of finite amplitude. J Acoust Soc Am 1997;101:1298–1308.

Krouskop TA, Dougherty DR, Levinson SF. A pulsed Doppler ultrasonic system for making non-invasive measurements of the mechanical properties of soft tissue. J Rehabil Res Dev 1987;24:1–8.

Landau LD, Liftshitz EM. Theory of elasticity. Moscow: Nauka, 1965.
Lerner R.M, Huang SR, Parker KJ. Sonoelasticity images derived from ultrasound signals in mechanically vibrated tissues. Ultrasound Med Biol 1990;16:231–239.
Manduca A, Muthupillai R, Rossman PJ, Greenleaf JF, Ehman RL. Local wavelength estimation for magnetic resonance elastography. In: Proceedings of International Conference on Image Processing. New York: IEEE, 1996:527–530.
Muthupillai R, Lomas DJ, Rossman PJ, et al. Magnetic resonance elastography by direct visualization of propagating acoustic strain waves. Science 1995;269:1854–1857.
Novikov BK, Rudenko OV, Timoshenko VI. Nonlinear underwater acoustics. New York: American Institute of Physics, 1987.
O'Donnell M, Skovoroda AR, Shapo BM, Emelianov SY. Internal displacement and strain imaging using ultrasonic speckle tracking. IEEE Trans Ultrason Ferroelectr Freq Contr 1994;41:314–325.
Ophir J, Cespedes I, Ponnekanti HL, Yazdi Y, Li X. Elastography: A quantitative method for imaging the elasticity of biological tissues. Ultrason Imaging 1991;13:111–117.
Ophir J, Cespedes I, Garra B, et al. Elastography: Ultrasonic imaging of tissue strain and elastic modulus in vivo. Eur J Ultrasound 1996;3:49–70.
Parker KJ, Huang SR, Musulin RA, Lerner RM. Tissue response to mechanical vibrations for "sonoelasticity imaging." Ultrasound Med Biol 1990;16:241–246.
Patton CA, Harris GR, Phillips RA. Output levels and bioeffects indices from diagnostic ultrasound exposure data reported to the FDA. IEEE Trans Ultrason Ferroelectr Freq Contr 1995;41:353–359.
Plewes DB, Betty I, Urchuk SN, Soutar I. Visualizing tissue compliance with MR imaging. J Magn Reson Imag 1995;5:733–738.
Rudenko OV. Nonlinear sawtooth-like waves. Physics-Uspehkhi 1995; vol. 38, pp. 965–989.
Rudenko OV, Soluyan SI. Theoretical foundations of nonlinear acoustics. New York: Plenum, 1977.
Rudenko OV, Soluyan SI, Khokhlov RV. Problems of the theory of nonlinear acoustics. In: L. Bjorno, ed. Finite-amplitude wave effects in fluids. London: IPC Science and Technology Press Ltd., 1974; 92–98.
Rudenko OV, Sagatov MM, Sapozhnikov OA. Thermal self-focusing of sawtooth waves. Sov Phys JETP 1990;71:449–454.
Rudenko OV, Sarvazyan AP, Emelianov SY. Acoustic radiation force and streaming induced by focused nonlinear ultrasound in a dissipative medium. J Acoust Soc Am 1996;99:2791–2798.
Sarvazyan AP. Low frequency acoustical characteristics of biological tissues. Mech Polymers 1975;4:691–695.
Sarvazyan AP. A new approach to remote ultrasonic evaluation of viscoelastic properties of tissues for diagnostics and healing monitoring. Abstract of ARPA/ONR Medical Ultrasonic Imaging Technology Workshop, Landsdowne, Virginia, January 24–26, 1995a.
Sarvazyan AP, Skovoroda AR, Emelianov SY, et al. Biophysical bases of elasticity imaging. In: Jones JP, ed. Acoustical Imaging 21. New York: Plenum Press, 1995b;223–240.
Sarvazyan AP, Emelianov SY, Lubinski MA, et al. Multipurpose ultrasound transducers for elasticity imaging. In: Proceedings of Office of Naval Research (DOD, Department of Navy) Workshop on Perspectives of Ultrasonic Imaging Transducers, April 30–May 4, 1995, Elvetham Hall, Basingstoke, UK, 1995c.
Sarvazyan AP. Method and device for shear wave elasticity imaging. US Patent Number 5,606,971. 1997.
Sarvazyan AP, Rudenko OV. Shear Wave Elasticity Imaging. In: Proceedings World Congress on Ultrasonics, August 1997, Yokohama, Japan, 1997.
Skovoroda AR, Emelianov SY, Lubinski MA, Sarvazyan AP, O'Donnell M. Theoretical analysis and verification of ultrasound displacement and strain imaging. IEEE Trans Ultrason Ferroelectr Freq Contr 1994;41:302–313.
Skovoroda AR, Emelianov SY, O'Donnell M. Tissue elasticity reconstruction based on ultrasonic displacement and strain imaging. IEEE Trans Ultrason Ferroelectr Freq Contr 1995;42:747–765.
ter Haar G. Ultrasonic biophysics. In: Hill CR, ed. Physical principles of medical ultrasonics. Chichester: Ellis Horwood Limited, 1986; 379–435.
Vinogradova MB, Rudenko OV, Sukhorukov AP. Theory of waves, 2nd ed. Nauka: Moscow, 1990 (in Russian).
Yamakoshi Y, Sato J, Sato T. Ultrasonic imaging of the internal vibration of soft tissue under forced vibration. IEEE Trans Ultrason Ferroelectr Freq Contr 1990;37:45–53.
Young YA, Axel L, Dougherty L, Bogen DK, Parenteau CS. Validation of tagging with MR imaging to estimate material deformation. Radiology 1993;188:101–108.
Zerhouni EA, Parish DM, Rogers WJ, Yang A, Shapiro EP. Human heart: Tagging with MR imaging—A method for noninvasive assessment of myocardial motion. Radiology 1988;169:164–172.